

# Mo(IV) and W(IV) cyanido complexes with Schiff bases. Synthesis, X-ray single crystal structures, physicochemical properties and quantum chemical calculations



Janusz Szklarzewicz<sup>\*</sup>, Michael Skaisgirski<sup>1</sup>, Patrycja Paciorek, Katarzyna Kurpiewska, Piotr Zabierowski, Mariusz Radoń

Faculty of Chemistry, Jagiellonian University, R. Ingardena 3, 30-060 Kraków, Poland

## ARTICLE INFO

### Article history:

Received 23 April 2013

Accepted 2 July 2013

Available online 24 October 2013

### Keywords:

Salicylaldehyde  
Cyanido complexes  
Molybdenum  
Tungsten  
Crystal structure  
Cyclic voltammetry

## ABSTRACT

In the reaction of salicylaldehyde derivatives and aminoethanol with Mo(IV) or W(IV) cyanido complexes, six new salts were isolated and characterized by physicochemical measurements. The single crystal X-ray analysis of four salts of the formula  $(PPh_4)_2[M(CN)_3O(LL)] \cdot nH_2O$ , (where LL = Schiff bases formed *in situ* in the reaction of aminoethanol and 5-bromo-, 5-chloro-, 5-methoxy-, 3,5-dichloro- or 5-bromo-3-methoxy-substituted salicylaldehyde, M = Mo or W,  $n = 1, 1.5, 2$  or 5 water molecules) reveals a distorted octahedral geometry of the anions. All the complexes were characterized by elemental analysis, IR and UV–Vis spectroscopy and by cyclic voltammetry measurements. The role of the salicylaldehyde substituents on the structures and physicochemical properties is discussed. The results are compared with quantum chemical calculations, indicating that, contrary to literature data, even strong hydrogen bonds do not influence the anion structure.

© 2013 Elsevier Ltd. All rights reserved.

## 1. Introduction

The structures of anions (or cations) of d-electron metal complexes are very often discussed in terms of ligand–metal interactions (for example the *trans* effect), but they also serve as an interesting source of information for the interactions of complex cations (or anions) with solvent molecules. During the last few years, much attention has been directed towards the syntheses of Mo(IV) and W(IV) oxido-cyanido complexes as these complexes are especially good for structure discussions due to their octahedral structures with fixed ligand positions [1]. In complexes with  $[M(CN)_4OL]^{n-}$  anions (M = Mo or W, L denotes a monodentate ligand) the ligand L is always *trans* to the M=O bond. In complexes with  $[Mo(CN)_3O(LL)]^{n-}$  anions (LL denotes a bidentate ligand) one end of LL ligand is also *trans* to the M=O bond, while the second donor atom is in a *cis* position. The stability of the complex structure is very promising for an investigation of the correlations between the structure and physicochemical properties.

The main problem is that for molybdenum(IV) and tungsten(IV) cyanido complexes only a few complexes are known, especially

with organic ligands [2–20]. Many efforts were undertaken to synthesize new complexes of this type, but still less than 50 were known, until now. The number of crystal structures resolved is even smaller, which makes systematic comparisons not always possible. Thus, it is difficult to draw correlations between the ligand and physicochemical properties for a given complex. It is known, however, that complexes with the same anion and different cations show anion distortion, discussed mainly in terms of possible long range hydrogen interactions influencing the anion structure [1].

In this work we synthesized several new complexes of Mo(IV) and W(IV) with Schiff base ligands derived from salicylaldehyde and 2-aminoethanol. To study the small effects of ligand and solvent interactions we decided to use substituted salicylaldehydes. The selected Schiff bases are identical to those used by us for copper(II) complexes (with 5-chloro, 5-bromo and 5-bromo-3-methoxy substituents), but the list of substituents was increased to include 3,5-dichloro and 5-methoxy [21]. It has been found that small changes on these ligands can dramatically influence the long distance interactions for copper complexes, even by changing the copper coordination number, which was interpreted in terms of hydrogen bonding effects. However, for 4- and 5-d electron metals, the hydrogen bonding interactions may not be so important as is suggested for 3-d metals. We also carried out quantum chemical calculations for isolated complex anions to examine if the observed deformation of the Mo(IV) or W(IV) anion may be reproduced

<sup>\*</sup> Corresponding author. Tel.: +48 12 6632231; fax: +48 12 6340515.

E-mail addresses: [szklarze@chemia.uj.edu.pl](mailto:szklarze@chemia.uj.edu.pl), [janusz.szklarzewicz@uj.edu.pl](mailto:janusz.szklarzewicz@uj.edu.pl) (J. Szklarzewicz).

<sup>1</sup> On leave from the Institut für Anorganische und Analytische Chemie, Albert-Ludwigs-Universität Freiburg, Albertstr. 21, 79104 Freiburg, Germany.

without considering the hydrogen bonding network present in the crystal structure.

## 2. Experimental

### 2.1. Materials and methods

$K_3Na[Mo(CN)_4O_2] \cdot 6H_2O$  and  $K_3Na[W(CN)_4O_2] \cdot 6H_2O$  were synthesized according to the literature methods [22,16]. All other chemicals were of analytical grade (Aldrich) and were used as supplied. Microanalyses of carbon, hydrogen and nitrogen were performed using a Vario Micro Cube elemental analyzer. Solid samples for IR spectroscopy were compressed as KBr pellets and the IR spectra were recorded on a Bruker EQUINOX 55 FT-IR spectrophotometer. Electronic absorption spectra (qualitative) were measured with a Shimadzu UV-Vis-NIR UV-3600 spectrophotometer. Diffuse reflectance spectra were measured in  $BaSO_4$  pellets with an ISR-3100 attachment. Cyclic voltammetry measurements were carried out in DMSO (dimethyl sulfoxide) with  $[Bu_4N]PF_6$  (0.10 M) as the supporting electrolyte, using Pt working and counter and Ag/AgCl reference electrodes on an AUTOLAB/PGSTAT 128 N Potentiostat/Galvanostat.  $E_{1/2}$  values were calculated from the average anodic and cathodic peak potentials,  $E_{1/2} = 0.5(E_a + E_c)$ . The redox potentials were calibrated versus ferrocene (0.440 V versus SHE), which was used as an internal potential standard for measurements in organic solvents to avoid the influence of a liquid

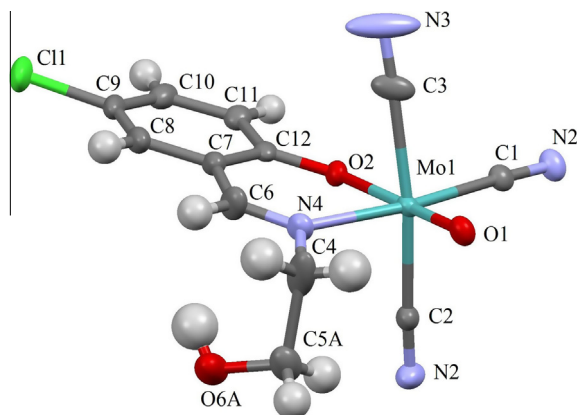


**Fig. 1.** Structure of the  $[Mo(CN)_3O(clsb)]^{2-}$  ion in **2a** with the atom labelling scheme and 50% displacement ellipsoids.

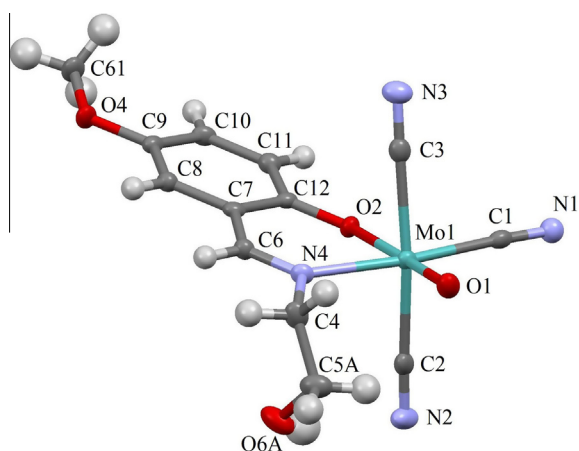


**Fig. 2.** Structure of the  $[Mo(CN)_3O(metsb)]^{2-}$  ion in **3** with the atom labelling scheme and 50% displacement ellipsoids.

junction potential; the final values are reported versus the standard hydrogen electrode (SHE).

### 2.2. Theoretical calculations

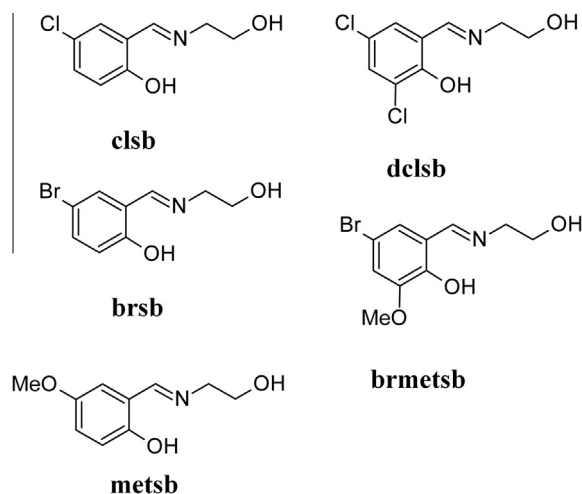
Quantum chemical calculations were performed using Turbomole 5.9 [23] and GAUSSIAN 09 [24] packages. The structures of the isolated  $[Mo(CN)_3O(LL)]^{2-}$  anions (without counterions) were optimized in Turbomole at the DFT:B3LYP/def2-TZVP level, both in the gas phase and in a conductor-like screening model (COSMO) with  $\epsilon = 4$ . In the case of **3**, the torsion angle C4–C5–O3–H3A (see Fig 2) was constrained to its value found in the crystal structure in order to prevent spurious rotation of the C–CH<sub>2</sub>OH group leading to the formation of intramolecular hydrogen bonding with one of the CN ligands (which is not present in the crystal structure and thus should be considered as an artifact of the present simple model, not accounting for the environment of the  $[M(CN)_3O(LL)]^{2-}$  anions). Mulliken and Hirshfeld atomic charges on the phenolic O atom of each LL ligand were obtained from single-point DFT:B3LYP/6-31G(d) calculations with GAUSSIAN 09, performed for the isolated LL<sup>−</sup> fragments at their geometries cut from the previously optimized  $[Mo(CN)_3O(LL)]^{2-}$  structures.

### 2.3. Synthesis

The ligands used in the synthesis are presented in Scheme 1. They were synthesized *in situ* by the reaction of the appropriate substituted salicylaldehyde and aminoethanol. The formed Schiff bases were denoted as Hclsb, Hbrsb, Hmetsb, Hdclsb and Hbrmetsb for 5-chloro-, 5-bromo-, 5-methoxy-, 3,5-dichloro- and 5-bromo-3-methoxy-salicylaldehyde, respectively.

#### 2.3.1. Synthesis of $[PPh_4]_2[Mo(CN)_3O(brsb)] \cdot 3H_2O$ (**1**)

2-Aminoethanol (39  $\mu$ l, 0.650 mmol) and 5-bromosalicylaldehyde (130.6 mg, 0.650 mmol) in 15 cm<sup>3</sup> ethanol were refluxed for 10 min. The solution was cooled to room temperature and a solution of  $K_3Na[Mo(CN)_4O_2] \cdot 6H_2O$  (378.8 mg, 0.788 mmol) in 25 cm<sup>3</sup> water was added. The reflux was continued for 20 min. Thereafter tetraphenylphosphonium chloride (750.0 mg, 2.00 mmol) was added and the solution was left for crystallization. After a few hours sparkling dark green crystals were obtained. The compound was filtered, washed with water and dried in air. Yield 673.6 mg, 87%. MW 1165.89. *Anal. Calc.* for  $C_{60}H_{55}BrMoN_4O_6P_2$ : C, 61.81; H, 4.75; N 4.81. Found: C, 62.16; H, 4.565; N, 4.96%.



**Scheme 1.**

### 2.3.2. Synthesis of $[PPh_4]_2[Mo(CN)_3O(cisb)] \cdot 2H_2O$ (**2**)

The synthetic procedure was identical as for **1**, but as the aldehyde 5-chlorosalicylaldehyde (102.0 mg, 0.650 mmol) was used. Some of the dark green crystals formed were kept in the mother liquor for crystal analysis (salt **2a**) while the rest were filtered off, washed with water and dried in air. Salts **2** and **2a** (dark green) were solvatomorphs. Yield 123.0 mg, 16%. MW 1103.53. *Anal. Calc.* for  $C_{60}H_{53}ClMoN_4O_5P_2$ : C, 65.31; H, 4.84; N, 5.08. Found: C, 65.57; H, 4.838; N, 5.07%.

### 2.3.3. Synthesis of $[PPh_4]_2[Mo(CN)_3O(metsb)] \cdot 5H_2O$ (**3**)

The synthetic procedure was identical as for **1**, but as the aldehyde 5-methoxysalicylaldehyde (81  $\mu$ l, 0.650 mmol) was used. Yield 174.6 mg, 23%. MW 1153.03. *Anal. Calc.* for  $C_{61}H_{62}MoN_4O_9P_2$ : C, 63.54; H, 5.42; N, 4.86. Found: C, 63.37; H, 5.386; N, 4.85%.

### 2.3.4. Synthesis of $[PPh_4]_2[W(CN)_3O(brmetsb)] \cdot 1.25H_2O$ (**4**)

2-Aminoethanol (60  $\mu$ l, 1.00 mmol) and 5-bromo-3-methoxysalicylaldehyde (152.1 mg, 0.658 mmol) in 15 cm<sup>3</sup> ethanol were refluxed for 10 min. The solution was cooled to room temperature and a solution of  $K_3Na[W(CN)_4O_2] \cdot 6H_2O$  (568.3 mg, 1.00 mmol) in 37.5 cm<sup>3</sup> water was added. Additionally 2 M HCl (400  $\mu$ l) was added, too. The reflux was continued for 20 min. Thereafter a warm solution of tetraphenylphosphonium chloride (562.3 mg, 1.5 mmol) in 30 cm<sup>3</sup> water was added and the solution was left for crystallization. After a few hours sparkling violet crystals were obtained. The compound was filtered, washed with water and dried in air. Yield: 131.9 mg, 16%. MW 1256.80. *Anal. Calc.* for  $C_{61}H_{54}BrWN_4O_{5.25}P_2$ : C, 58.30; H, 4.33; N, 4.46. Found: C, 58.10; H, 4.288; N, 4.36%.

### 2.3.5. Synthesis of $[PPh_4]_2[Mo(CN)_3O(dclsb)] \cdot H_2O$ (**5**)

2-Aminoethanol (30  $\mu$ l, 0.501 mmol) and 3,5-dichlorosalicylaldehyde (96.9 mg, 0.507 mmol) in 7.5 cm<sup>3</sup> ethanol were refluxed for 10 min. The solution was cooled to room temperature and a solution of  $K_3Na[Mo(CN)_4O_2] \cdot 6H_2O$  (245 mg, 0.510 mmol) in 19 cm<sup>3</sup> water as well as 2 M HCl (0.1 ml) were added. The reflux was continued for 15 min. Thereafter a solution of tetraphenylphosphonium chloride (284 mg, 0.758 mmol) in 15 cm<sup>3</sup> water was added and the solution was left for crystallization. After a few hours, very small black sparkling crystals were obtained. The

compound was filtered, washed with water three times and dried in air. Yield: 135.6 mg, 24%. MW 1119.8. *Anal. Calc.* for  $C_{60}H_{50}Cl_2MoN_4O_4P_2$ : C, 64.35; H, 4.50; N, 5.00. Found: C, 64.17; H, 4.45; N, 4.97%.

### 2.3.6. Synthesis of $[PPh_4]_2[Mo(CN)_3O(brmetsb)] \cdot 2H_2O$ (**6**)

2-Aminoethanol (60  $\mu$ l, 1.00 mmol) and 5-bromo-3-methoxysalicylaldehyde (153 mg, 0.662 mmol) in 10 cm<sup>3</sup> ethanol were refluxed for 10 min. The solution was cooled to room temperature and a solution of  $K_3Na[Mo(CN)_4O_2] \cdot 6H_2O$  (497 mg, 1.03 mmol) in 25 cm<sup>3</sup> water was added. The reflux was continued for 15 min. Thereafter a solution of tetraphenylphosphonium bromide (803 mg, 1.92 mmol) in 20 cm<sup>3</sup> water was added and the solution was left for crystallization. After a few hours, black sparkling crystals were obtained. The compound was filtered, washed with water three times and dried in air. Yield: 642 mg, 87%. MW 1119.8. *Anal. Calc.* for  $C_{61}H_{55}BrMoN_4O_6P_2$ : C, 62.20; H, 4.71; N, 4.76. Found: C, 62.30; H, 4.52; N, 4.65%.

## 2.4. Crystallographic data collection and structure refinement

Crystals of **2a**, **3** and **4** suitable for X-ray analysis were selected from the materials prepared as described in the Experimental Section. Intensity data were collected on a SuperNova diffractometer (Agilent Technologies) at 110–113 K, equipped with an Atlas detector and a microfocus Mo  $K\alpha$  ( $\lambda = 0.71073$  Å) radiation source operating at 50 kV and 1 mA for **2a**, **3** and **4**. Data were processed using CRYALIS<sup>Pro</sup>. The crystal data and details of data collection and structure refinement parameters are summarized in Table 1. The positions of most of the atoms were determined by direct methods (SIR-97) [25], whilst other non-hydrogen atoms were located on difference Fourier maps. Most of the non-hydrogen atoms were refined anisotropically using weighted full-matrix least-squares on  $F^2$ . Atoms that exhibited disorder were refined isotropically. All hydrogen atoms bonded to carbon were included in the structure factor calculations at idealized positions. The structures were refined by the SHELXL program [26]. Structural description graphics were prepared with the program Mercury 3.0.

**Table 1**  
Crystal data and structure refinement parameters for **2a**, **3** and **4**.

	<b>2a</b>	<b>3</b>	<b>4</b>
Empirical formula	$C_{60}H_{59.5}ClMoN_4O_{8.25}P_2$	$C_{61}H_{62}MoN_4O_9P_2$	$C_{61}H_{54}BrWN_4O_{5.25}P_2$
Formula weight	1162.48	1153.03	1252.78
Crystal size (mm)	0.55 × 0.2 × 0.15	0.4 × 0.2 × 0.15	0.1 × 0.1 × 0.35
Crystal system	triclinic	triclinic	monoclinic
Space group	$P\bar{1}$	$P\bar{1}$	$P2_1/n$
<i>a</i> (Å)	12.597(5)	12.083(5)	9.83510(10)
<i>b</i> (Å)	14.203(5)	13.815(5)	23.8400(3)
<i>c</i> (Å)	17.232(5)	18.024(5)	23.6775(3)
$\alpha$ (°)	73.398(5)	72.898(5)	90.00
$\beta$ (°)	72.505(5)	75.469(5)	98.4180(10)
$\gamma$ (°)	85.310(5)	85.204(5)	90.00
<i>V</i> (Å <sup>3</sup> )	2817.8(17)	2783.5(17)	5491.82(11)
<i>Z</i>	2	2	4
<i>T</i> (K)	113(5)	110(10)	110(2)
<i>D<sub>c</sub></i> (Mg/m <sup>3</sup> )	1.374	1.376	1.515
$\mu$ (mm <sup>-1</sup> )	0.396	0.354	2.943
Reflections measured	40586	24537	27552
Reflections unique	12648	11953	11371
Reflections observed [ $I > 2\sigma(I)$ ]	10643	9990	9734
$R_1[F^2 > 2\sigma(F^2)]^a$	0.0354	0.0371	0.0272
$wR_2(F^2)^a$	0.0802	0.0928	0.0533
<i>S</i>	1.033	1.013	1.034

<sup>a</sup>  $w = 1/[\sigma^2(F_o^2) + (0.0297P)^2 + 0.0712P]$  where  $P = (F_o^2 + 2F_c^2)/3$ ,  $R_1 = \sum(|F_o| - |F_c|)/\sum(|F_o|)$  and  $wR_2 = (\sum[w(F_o - F_c)^2])^{1/2}$ .

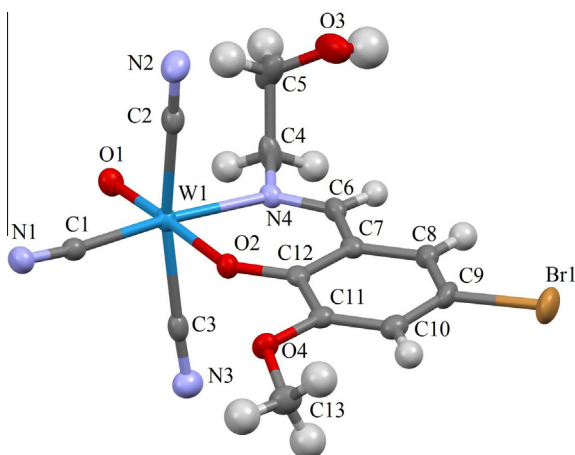


Fig. 3. Structure of the  $[W(CN)_3O(brmetsb)]^{2-}$  ion in **4** with the atom labelling scheme and 50% displacement ellipsoids.

### 3. Results and discussion

#### 3.1. Crystal structures

The asymmetric part of the unit cell in the crystal structures of **2a**, **3** and **4** contain the anion, two cations and water molecules. The anions are shown in Figs. 1–3 (in those figures hydrogen atoms are omitted for clarity). Selected bond lengths and angles for the determined crystal structures of **2a**, **3** and **4** are listed in Table 2.

The organic ligand coordinates in a bidentate mode to afford a distorted octahedral geometry with three cyanido ligands and a nitrogen atom of the Schiff base in the equatorial positions, and with the oxido ligand and the phenolic oxygen occupying the axial positions.

The anions are distorted: the average O1–M–O angle is  $176.69^\circ$  and the average C1–M–O1 and N4–M–O1 angles are  $93.68^\circ$  and  $97.44^\circ$ , respectively. A similar type of deformation is observed for all Mo(IV) and W(IV) complexes of the  $[M(CN)_3O(LL)]^{n-}$  ( $n = 1$  or  $2$ ) type known to date [1,18,7,19,20,27]. The highest distortion, with the O–Mo–O angle equal to  $164.30^\circ$ , was found for the

Table 2

Selected bond lengths [Å] and angles [ $^\circ$ ] for  $[PPh_4]_2[Mo(CN)_3O(clusb)] \cdot 5H_2O$  (**2a**),  $[PPh_4]_2[Mo(CN)_3O(metsb)] \cdot 5H_2O$  (**3**) and  $[PPh_4]_2[W(CN)_3O(brmetsb)] \cdot 1.5H_2O$  (**4**) with estimated standard deviations in parentheses. M = Mo or W.

	2a	3	4
<i>Bond lengths</i>			
M=O1	1.694(2)	1.695(2)	1.727(2)
M–O2	2.086(2)	2.069(2)	2.072(2)
M–N4	2.184(2)	2.198(2)	2.132(2)
M–C1	2.160(2)	2.162(3)	2.144(3)
M–C2	2.193(3)	2.207(3)	2.187(3)
M–C3	2.200(3)	2.201(3)	2.172(3)
C1–N1	1.153(2)	1.159(3)	1.156(3)
C2–N2	1.154(4)	1.157(3)	1.153(4)
C3–N3	1.147(5)	1.156(3)	1.154(4)
<i>Bond angles</i>			
N4–M–O2	81.76(7)	81.61(7)	82.83(8)
O1–M–O2	176.69(7)	175.67(7)	177.49(7)
C1–M–N4	168.90(8)	170.11(7)	167.55(10)
C2–M–C3	168.44(9)	169.95(8)	167.93(11)
O1–M–N4	95.38(8)	94.44(8)	99.63(9)
O1–M–C1	95.70(8)	95.41(8)	92.64(10)
C2–M–N4	92.43(9)	91.87(9)	85.78(9)
C3–M–N4	85.86(10)	87.18(8)	89.34(9)
C1–M–O2	87.14(7)	88.52(7)	84.92(9)
C2–M–O2	85.59(7)	85.88(7)	83.07(9)
C3–M–O2	82.86(8)	84.08(7)	85.38(9)

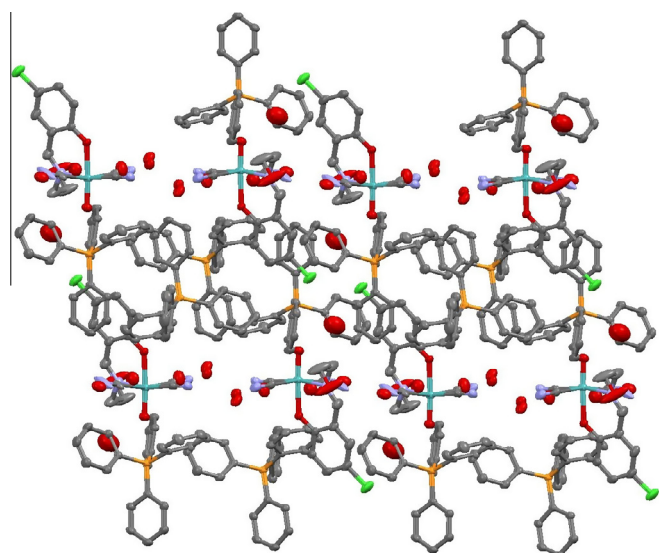


Fig. 4. The arrangement with distinguishable layers of anions and cations in **2a**.

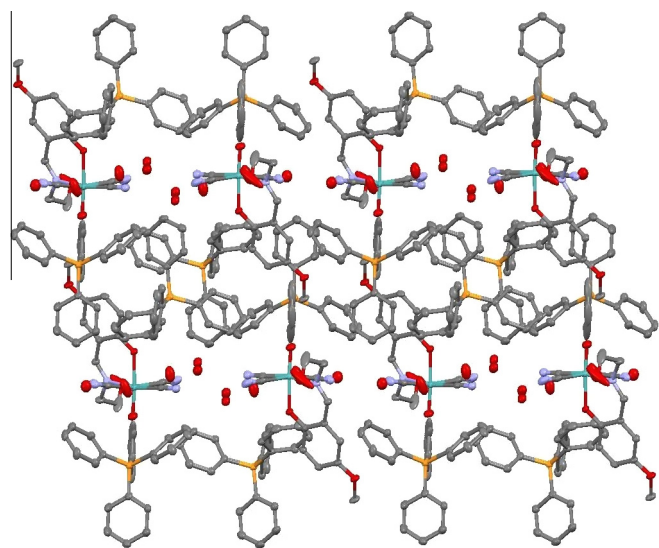


Fig. 5. The arrangement with distinguishable layers of anions and cations in **3**.

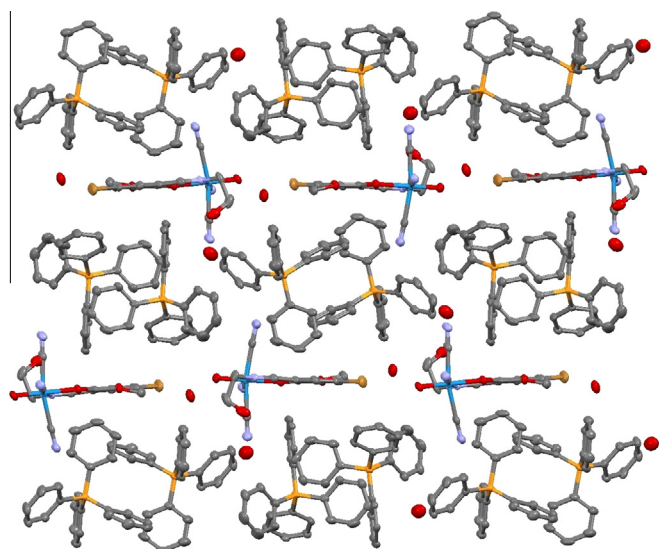
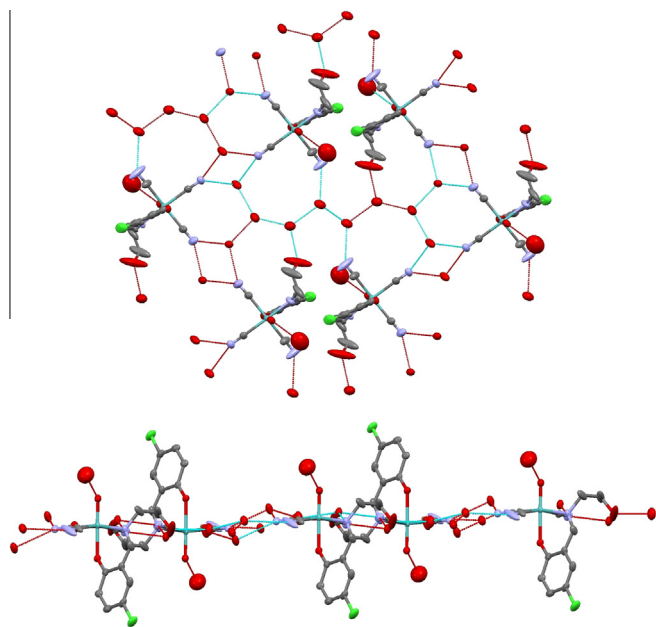


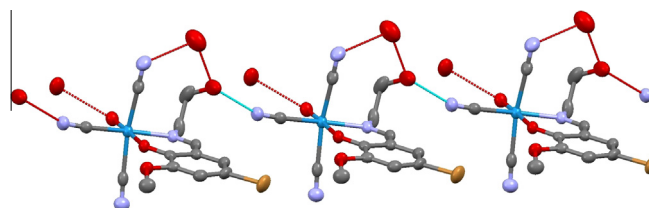
Fig. 6. The arrangement with distinguishable layers of anions and cations in **4**.

Fig. 7. Hydrogen bonding network in **2a**.

[PPh<sub>4</sub>]<sub>2</sub>[Mo(CN)<sub>3</sub>O(pzac)]·2H<sub>2</sub>O complex [27]. The average M–C and C≡N bond distances are 2.171 and 1.150 Å, respectively and these are very close to those found in the structure of the [Mo(CN)<sub>3</sub>O(pic)]<sup>2-</sup> anion, where the bond lengths are 2.161 and 1.148 Å, respectively [18]. The cyanido ligands are not bound with the same strength, usually the M–C bond *trans* located to the Mo–N is the shortest, whilst its C≡N bond is the longest.

The crystal packing of complexes **2a–4** are shown in Figs. 4–6. It can be seen that in the case of all the salts the layers of cations are separated by the layers of anions. Thus, there are no significant differences in the long distance packing.

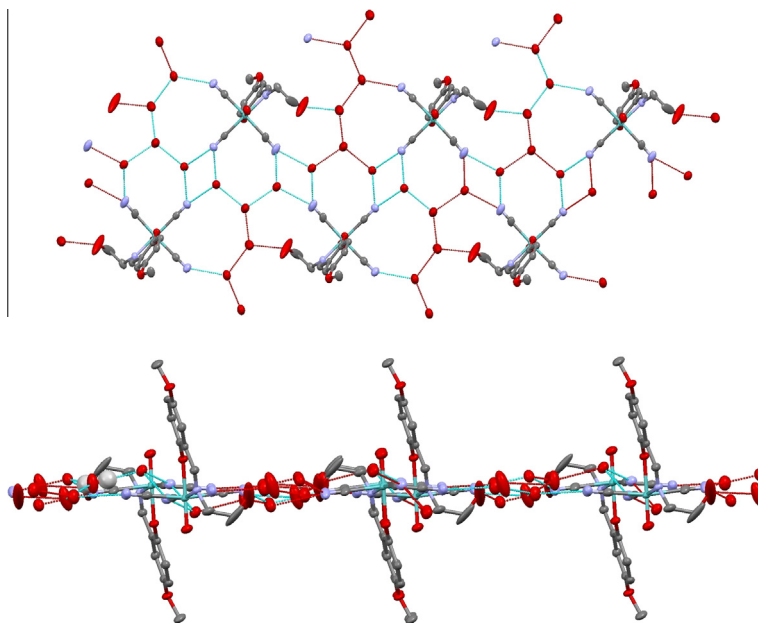
The anions and cations are bonded by a network of hydrogen bonds, as presented in Figs. 7–9. Selected bond lengths are given in Table 3. In **2a** all the cyanido ligands and O1 are involved in a three dimensional network presented in Fig. 7. The two cyanido ligand's nitrogens (N1 and N2) form double bridges with water mol-

Fig. 9. Hydrogen bonding network in **4**.

**Table 3**  
The hydrogen bond parameters in salts **2a–4**.

Complex	D–A	<i>d</i> (D–A) (Å)	DHA (°)
<b>2a</b>	N1–O22	2.914	177.59
	N1–O22'	2.970	173.99
	N2–O21	3.001	174.33
	N2–O21'	2.926	164.06
	N3–O23	3.034	176.12
	O1–O26	2.790	–
	O22–O25	2.780	173.03
	O21–O25	2.771	161.71
	O23–O24	2.757	164.96
	O24–O25	2.712	166.51
O24–O3	2.759	167.41	
<b>3</b>	N1–O21	2.950	168.33
	N1–O21'	2.936	174.18
	N2–O24	2.933	159.18
	N2–O24'	3.013	177.30
	N3–O25	3.019	167.95
	O21–O23	2.719	179.21
	O23–O24	2.855	168.63
	O22–O25	2.807	163.25
O22–O23	2.559	163.81	
<b>4</b>	N1–O3	2.810	168.93
	N2–O22	2.706	–
	O22–O3	2.772	–
	O1–O21	2.879	177.48

ecules, which form further water–water hydrogen bonds, yielding a plane structure of the anions. Every second Mo=O oxygen as well as every second organic ligand is located above or below the plane,

Fig. 8. Hydrogen bonding network in **3**.

as shown in the bottom part of Fig. 7. A very reach network of hydrogen bonds was found in **2a**, therefore relatively large separations of the anions are observed in the structure. This kind of layer arrangement is probably responsible for the easy dehydration of **2a** into **2**, when three water molecules are released. The repeated synthesis and analysis indicated only two water molecules in dried samples of **2**, while crystals kept in solution (**2a**) remain pentahydrated.

In salt **3**, the hydrogen bonding network is essentially similar to that in **2a**, the main difference is that the O1 oxygen does not form hydrogen bonds with the water molecules, as shown in the bottom part of Fig. 8. In **4** the hydrogen bonds arrange the anions in chains and not in planes. The oxygen atom from the W=O bond forms a hydrogen bond with one water molecule, but nitrogen N3 from the cyanido ligand is not involved in such an interaction. The presented data for the hydrogen bonds in Table 3 reveal relatively strong interactions, the D–H–A angle falling in the 159–178° range.

**Table 4**

Comparison of experimental and calculated M=O and M–O (phenolic) bond distances and calculated charges on the O (phenolic) atom in the free ligands.

Bond distance (Å)		Salt		
		<b>2</b>	<b>3</b>	<b>4</b>
M=O	found	1.694	1.695	1.727
	calculated <sup>a</sup>	1.689 (1.694)	1.692 (1.698)	1.723 (1.729)
M–O (phenolic)	found	2.086	2.069	2.072
	calculated <sup>a</sup>	2.170 (2.127)	2.142 (2.101)	2.127 (2.103)
O (phenolic) charge <sup>b</sup>		–0.67	–0.69	–0.64
		(–0.43)	(–0.45)	(–0.41)

<sup>a</sup> Structures of isolated  $[M(CN)_3O(LL)]^{2-}$  anions optimized in the gas phase (in parenthesis in the COSMO model) at the DFT:B3LYP/def2-TZVP level.

<sup>b</sup> Mulliken (Hirshfeld) charge from single-point DFT:B3LYP/6-31G(d) calculations on each LL taken from the crystal structure of the respective salt.

As it can be seen in Table 2, the hydrogen bond formation has little influence on the M=O, M–C and C≡N bond lengths. For example in **3**, the oxygen atom in Mo=O does not form hydrogen bonds. Furthermore, this bond is the longest (1.739 Å) one, which is contrary to expectation, but it is still very close to the value in **4** (1.727 Å). Similarly, the N3 atom is either involved in single or no hydrogen bonds, which has no influence on the C–N bond distances for salts **2–4**.

There has been a long discussion on the influence of hydrogen bonds on the structure of  $[M(CN)_3O(LL)]^{n-}$  anions (M = Mo or W), especially the M=O bond distance, so far without definite conclusions [1,19]. Here, for the first time, we have obtained a series of compounds with similar organic ligands and very different hydrogen bonds patterns involving the O1 atom (M=O group). While in **3** this oxygen atom remains free, in **2a** and **4** it is involved in relatively strong hydrogen bonds with water molecules. Despite this profound difference, **2a** and **3** have nearly identical M=O distances (Table 4). Compound **4** has, clearly, a much longer M=O distance than **2** and **3** for it contains W instead of Mo.

Table 4 contains the M=O distances calculated at the DFT level in the gas-phase and in the COSMO model, as well as the experimental data. The purpose of the COSMO approach is to roughly simulate the effect of a polarizable environment in the condensed phase, which is completely neglected in standard (gas-phase) calculations. As can be seen in Table 4, the calculated M=O bond distances agree with experimental data very well, with discrepancies below 0.005 Å (the COSMO distances, being 0.005–0.006 Å shorter from the gas-phase ones, are closer to the experimental values). Given that both sets of calculations refer to isolated  $[M(CN)_3O(LL)]^{2-}$  anions, i.e. they completely neglect the intermolecular interactions occurring in the crystal structures, the good agreement between the calculations and the crystal structures goes in line with one of the conclusions above: the M=O distance is hardly affected by hydrogen bonding.

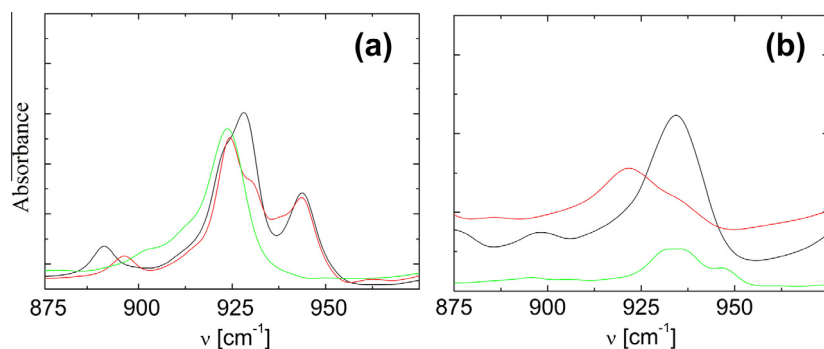


**Fig. 10.** IR spectra of a) **1** (black line), **2** (red line) and **3** (green line), b) **4** (red line), **5** (green line) and **6** (black line). Spectra measured in KBr in the 875–975  $\text{cm}^{-1}$  region. (Color online)

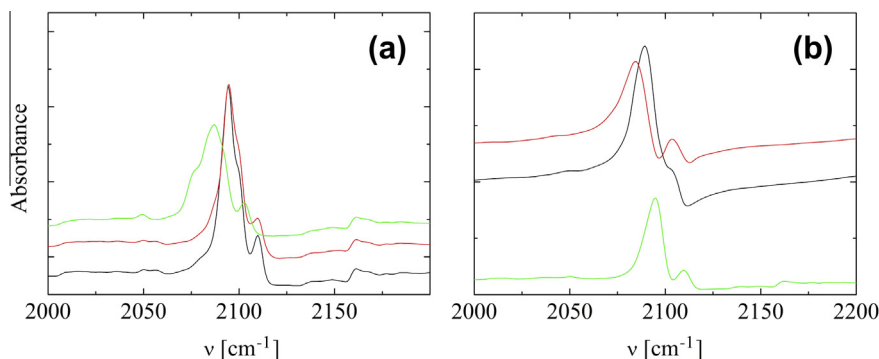


**Fig. 11.** IR spectra (in the 2000–2200  $\text{cm}^{-1}$  region) of a) **1** (black line), **2** (red line) and **3** (green line) b) **4** (red line), **5** (green line) and **6** (black line). (Color online)

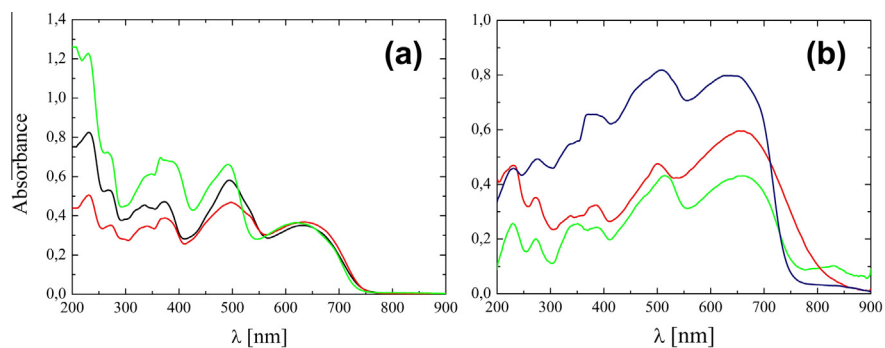


**Fig. 12.** The reflectance spectra of a) **1** (black line), **2** (red line) and **3** (green line) b) **4** (red line), **5** (green line) and **6** (blue line) after Kubelka–Munk transformation. BaSO<sub>4</sub> as internal standard. (Color online)

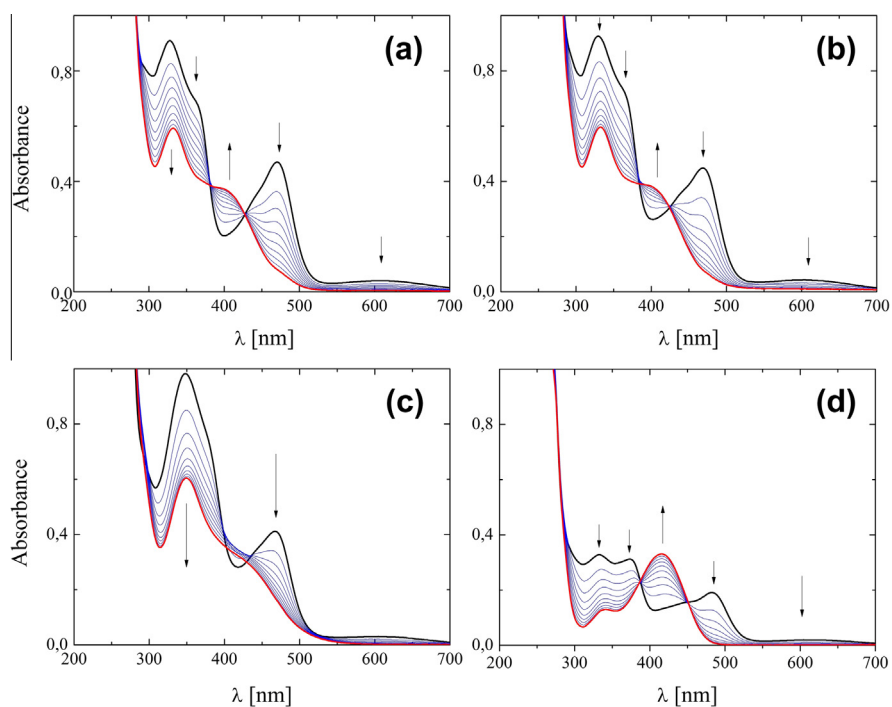


**Fig. 13.** UV-Vis spectra of **1** (a) **2** (b), **3**(c) and **5** (d) vs. time in ethanol.  $T = 25.7\text{ }^{\circ}\text{C}$ ,  $d = 1\text{ cm}$ , time intervals 180 s, 15 spectra measured, arrows indicate the direction of the changes.

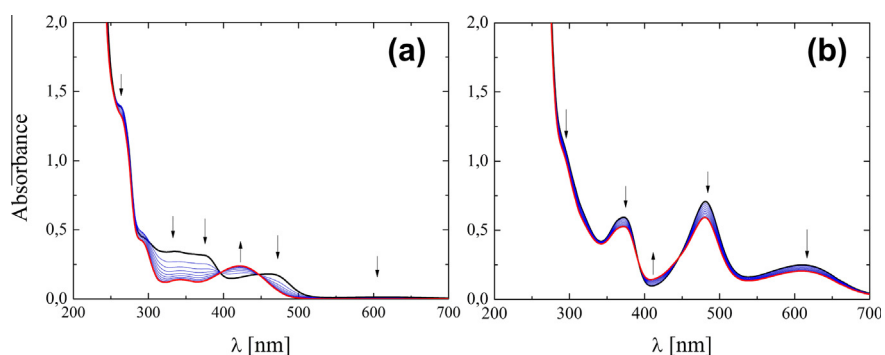


**Fig. 14.** UV-Vis spectra of **6** (a) and **4** (b) vs. time in ethanol.  $T = 25.7\text{ }^{\circ}\text{C}$ ,  $d = 1\text{ cm}$ , time intervals 180 s, 15 spectra measured, arrows indicate the direction of the changes.

Moreover, it seems that different LL ligands in compounds **1–3**, **5** and **6** point to very similar Mo=O distances. While experimental values are available only for **2** and **3**, the DFT ones can be computed for all of them, and they turn out to be very similar (gas-phase val-

ues for the remaining species: 1.688 Å for **1**, 1.686 Å for **5** and 1.688 Å for **6**). In contrast, the M–O (phenolic) bond distances show larger variations with respect to the organic ligand and also a worse agreement between the calculated and experimental values.

The M–O (phenolic) bond is a softer degree of freedom than the M=O distance, and thus it is presumably more affected by shortcomings of the computational method and the model used here (isolated anion). Nonetheless, the differences in the M–O (phenolic) bond distances between compounds **2–4** are nicely reproduced by the calculations, the DFT distances being systematically longer than the experimental ones (cf. Table 4). Interestingly, the M–O distance seems to be correlated with the atomic charge on the phenolic O atom: with increasing negative charge, the bonds become shorter.

### 3.2. IR spectra

The IR spectra of salts **1–6** are presented in Figs. 10 and 11 and are in agreement with the X-ray crystal structures for salts **2a–4**. The most interesting features for the Mo(IV) and W(IV) complexes are the  $\nu_{\text{M=O}}$  (in the 900–1000  $\text{cm}^{-1}$  range) and  $\nu_{\text{C}\equiv\text{N}}$  bands (in the 2050–2150  $\text{cm}^{-1}$  range). The  $\nu_{\text{M=O}}$  bands for salts **1–6** are observed at 928, 925, 924, 922, 934 and 934  $\text{cm}^{-1}$  respectively. Thus the studied substituents of the salicylaldehyde can be arranged for Mo(IV) complexes in order of increasing band energy as: 5-methoxy- < 5-chloro- < 5-bromo- < 3,5-dichloro- = 5-bromo-3-methoxy-. The  $\nu_{\text{C}\equiv\text{N}}$  bands for **1** are observed at 2094, 2098sh and 2110  $\text{cm}^{-1}$ , for **2** at 2095, 2098sh and 2110  $\text{cm}^{-1}$ , for **3** at 2077sh, 2087 and

2103  $\text{cm}^{-1}$ , for **4** at 2084 and 2104  $\text{cm}^{-1}$ , for **5** at 2095 and 2110  $\text{cm}^{-1}$  and for **6** at 2089 and 2103  $\text{cm}^{-1}$ . For the Mo(IV) complexes, the lowest energy band can be arranged in the series: 5-methoxy- < 5-bromo-3-methoxy- < 5-bromo- < 5-chloro- = 3,5-dichloro-, while the highest energy one can be divided in two groups:  $\nu_{\text{C}\equiv\text{N}} \sim 2103 \text{ cm}^{-1}$  for the salts with methoxy- and bromo-methoxysalicylaldehyde and  $\nu_{\text{C}\equiv\text{N}} \sim 2110 \text{ cm}^{-1}$  for the other salts.

### 3.3. UV–Vis spectra

The sample reflectance electronic spectra in the UV–Vis range for salts **1–3** are presented in Fig. 12. In general the spectra measured in the solid state for all the Mo(IV) complexes are similar (**1–6**). The lowest energy bands (at ca 650 nm) appear to be of *d–d* origin. In the reflectance spectra these forbidden transitions are well visible and their intensity is similar to the allowed transitions. However, for the Mo(IV) and W(IV) cyanido complexes with bidentate organic ligands the *d–d* transitions are overlapped with the charge-transfer ones which are also well visible in the spectra measured in solution.

The spectra in EtOH for all the complexes are presented in Figs. 13 and 14. The observed instability of the complexes in EtOH solution results in synthetic problems (low yield) and problems with recrystallisation of the complexes for structure measure-

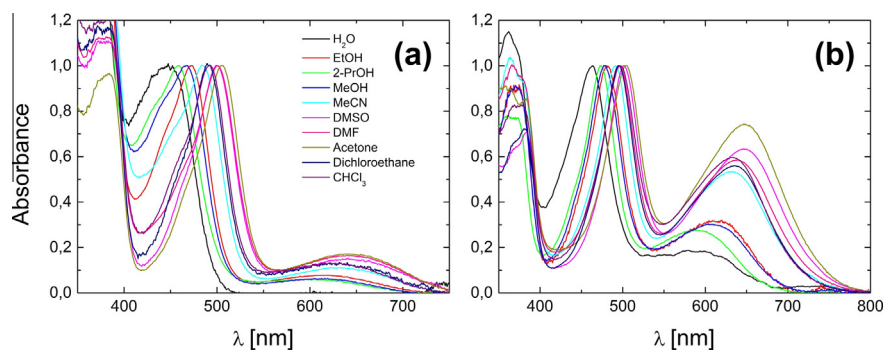


Fig. 15. The electronic spectra of **6** (a) and **4** (b) in different solvents. Qualitative spectra normalized for absorbance = 1 for the most intense CT band.  $T = 25 \text{ }^\circ\text{C}$ ,  $d = 1 \text{ cm}$ , qualitative spectra.

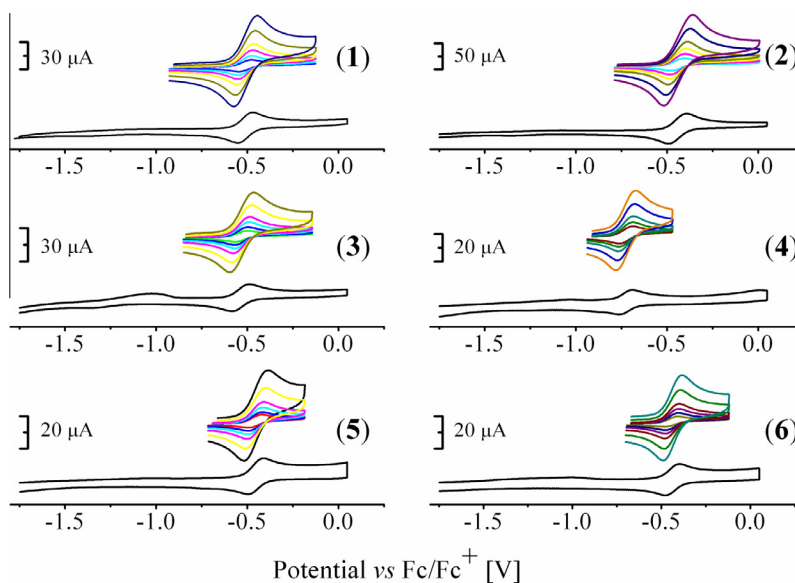


Fig. 16. The cyclic voltammetry of complexes **1–6** in DMSO. The overlaid curves above each main curve represent different potential scan rates – 20, 50, 100, 200, 500, 1000 mV/s with raising peak current, respectively. In the upper left corner a scale of current is presented.  $T = 25 \text{ }^\circ\text{C}$ , 20 mg of sample per 5 ml of solvent.

ments. To isolate salt **4** it was necessary to stabilize the aldehyde with excess of aminoethanol over aldehyde.

For a proper band assignment, the spectra in a series of organic solvents were also measured and are presented in Fig. 15 for Mo(IV) and W(IV) representatives, with the same LL ligand (salts **6** and **4**). The lowest energy bands (at ca. 600 nm) can be attributed to  $d-d$  transitions overlapped with MLCT (metal-to-ligand charge transfer) transitions. Such an assignment is in agreement with the literature data for  $[M(CN)_3O(LL)]^{n-}$  type ions and with the relatively low intensity of this band (for the Mo complexes) [1]. These bands are especially well visible in the reflectance spectra (see Fig. 12). For the Mo(IV) complexes (see for example the spectrum of salt **6** in Fig. 15) this band is almost solvent-independent, supporting its assignment as  $d-d$ . For the W salt (complex **4**) this band is much more intense ( $\epsilon_{615\text{ nm}} = 20.3 \pm 1.4 \times 10^2 \text{ mol}^{-1} \text{ dm}^3 \text{ cm}^{-1}$ , while for **6**  $\epsilon_{643\text{ nm}} = 705 \pm 10 \text{ mol}^{-1} \text{ dm}^3 \text{ cm}^{-1}$  in DMSO) and is solvent sensitive, indicating its stronger CT character. This is a typical behavior for similar W(IV) complexes [1].

The most intense band at ca. 500 nm has MLCT character and is strongly solvatochromic (Fig. 15). The molar extinction coefficients indicate allowed transitions (for example, salt **4**  $\epsilon_{485\text{ nm}} = 55 \pm 2 \times 10^2 \text{ mol}^{-1} \text{ dm}^3 \text{ cm}^{-1}$ , for **6**  $\epsilon_{615\text{ nm}} = 45 \pm 7 \times 10^2 \text{ mol}^{-1} \text{ dm}^3 \text{ cm}^{-1}$  in DMSO). The solvatochromism of  $[M(CN)_3O(LL)]^{n-}$  ions ( $M = \text{Mo}$  or  $\text{W}$ ) was investigated intensively earlier and support the MLCT character of the bands [28]. In the UV part of the spectra, bands attributed to intraligand transitions overlapped with anion ones are visible. The band closest to 400 nm is connected with the presence of the C=N bond and its position is typical for complexes with Schiff base ligands.

Solutions of complexes **1–6** are not very stable with time, as presented in Figs. 13 and 14. The most stable solutions are those in MeCN,  $\text{CHCl}_3$ , 1,2-dichloroethane and acetone. In other solvents a decrease of the bands is observed, connected with the organic ligand release. The process of ligand release in  $[M(CN)_3O(LL)]^{n-}$  type ions was studied earlier in detail for LL = picolinic acid or salicylaldehyde hydrazone and was used in a reaction mechanism study and in the synthesis of coordination isomers of Mo(IV) complexes [29].

#### 3.4. Cyclic voltammetry

The cyclic voltammograms for compounds **1–6** measured in DMSO are presented in Fig. 16. The redox potentials are included in Table 5. As can be seen in the Fig. 16, each of the synthesized complexes can be reversibly oxidized from  $[Mo(CN)_3O(LL)]^{2-}$  to  $[Mo(CN)_3O(LL)]^-$ . The redox potentials of the Mo(IV)/Mo(V) couple in the studied molybdenum complexes are influenced by the electron withdrawing effects of 5-substituents to a larger extent than 3-substituents. The potential-current transients for each complex for different potential scan rates indicate that the redox processes are diffusion controlled. Moreover, the anodic and cathodic potentials do not change significantly with the potential scan rates, which is associated with the reversibility of the studied redox sys-

**Table 5**

The cyclic voltammetry data for complexes **1–6** in DMSO. Potential sweep rate 100 mV/s,  $T = 298 \text{ K}$ . The redox potentials are reported vs.  $\text{Fc}/\text{Fc}^+$ .

Complex	$E_{1/2}$ (mV)	$\Delta E$ (mV)
<b>1</b>	–510	82
<b>2</b>	–444	92
<b>3</b>	–532	88
<b>4</b>	–726	78
<b>5</b>	–453	78
<b>6</b>	–439	73

tems. What is interesting is that we do not observe well defined cathodic waves at ca  $-1.3 \text{ V}$  attributed to the reduction of the ligands, as in the case of previously reported copper complexes [21].

The Mo(IV)/Mo(V) redox potential values determined herein lay in the range between the slightly lower value reported for the salicylaldehydehydrazone complex ( $-629 \text{ mV}$  versus  $\text{Fc}/\text{Fc}^+$  [13]) and the slightly higher value reported for the picolinic acid complex ( $-301 \text{ mV}$  versus  $\text{Fc}/\text{Fc}^+$  [18]). The difference between the redox potentials of the corresponding picolinic acid complexes of Mo(IV) and W(IV) is lower (117 mV lower value for the potential of the W(IV) complex) than that of the corresponding salicylidene-2-ethanolamine complexes **4** and **6** (287 mV).

These data indicate that the salicylaldehydehydrazone complexes of Mo(IV) are better reductants than the corresponding salicylidene-2-ethanolamine and picolinic acid complexes. What is more, the fourth oxidation state of tungsten is less stabilized in complexes with salicylidene-2-ethanolamine than with picolinic acid.

#### 4. Conclusions

The synthesized complexes of Mo(IV) and W(IV) with Schiff bases formed from aminoethanol and 5-bromo-, 5-chloro-, 5-methoxy-, 3,5-dichloro- and 5-bromo-3-methoxy-substituted salicylaldehyde, isolated as their tetraphenylphosphonium salts, belong to a very narrow class of compounds where changes in the aromatic ring substituents can influence the properties of the complexes. Quantum chemical calculations for the isolated complex anions show remarkable correlations between the calculated bond distances and those found by X-ray single crystal measurements, suggesting that the formation of even strong hydrogen bonds do not influence the structures of the complex anions considerably. Similarly, the calculated charge on phenolic oxygen is almost identical for all the complexes studied. On the other hand, the redox potentials of the complexes change strongly with the ligand substituent, by almost 0.1 V (between salt **6** and **3**). For substituents in the 5 position (complexes **1**, **2** and **3**) the  $E_{1/2}$  value increases in order: methoxy < bromo < chloro. In the same order, the increase of the  $d-d$  transition energy (Fig. 12) can also be observed. In the solid state, the substituents influence the IR spectra as well as the structures. This mainly results in a change of short contact interactions and also in the hydrogen bonding network formation. On the basis of all the presented data, it seems that for the 4th and 5th row elements, the main effect on the complex anion structure is metal and ligand type and not the network of hydrogen bonds. This is, however, very interesting, as substituents can be used to tune some physicochemical properties (like, for example, redox potentials) without changing the structure of the anion significantly.

#### Acknowledgment

M.R. thanks Foundation for Polish Science (FNP) for supporting his research work with the scholarship from the START program. The research was carried out with the equipment purchased thanks to the financial support of the European Regional Development Fund in the framework of the Polish Innovation Economy Operational Program (contract no. POIG.02.01.00-12-023/08). This work was supported in part by the Jagiellonian University.

#### Appendix A. Supplementary data

CCDC 934895, 934896 and 934897 contain the supplementary crystallographic data for complexes **4**, **3** and **2a**. These data can be obtained free of charge via <http://www.ccdc.cam.ac.uk/conts/retrieving.html>, or from the Cambridge Crystallographic Data

Centre, 12 Union Road, Cambridge CB2 1EZ, UK; fax: (+44) 1223-336-033; or e-mail: deposit@ccdc.cam.ac.uk.

## References

- [1] A. Samotus, J. Szklarzewicz, D. Matoga, *Bull. Pol. Acad. Sci., Chem.* 50 (2002) 145.
- [2] H. Arzoumanian, M. Pierrot, F. Ridouane, J. Sanchez, *Transition Met. Chem.* 16 (1991) 422.
- [3] H. Arzoumanian, A. Bouraoui, V. Lazzeri, M. Rajzmann, H. Teruel, *New J. Chem.* 16 (1992) 965.
- [4] D. Matoga, J. Szklarzewicz, A. Samotus, J. Burgess, J. Fawcett, D.R. Russell, *Polyhedron* 19 (2000) 1503.
- [5] A. Roodt, J.G. Leipoldt, S.S. Basson, I.M. Potgieter, *Transition Met. Chem.* 13 (1988) 336.
- [6] D. Matoga, J. Szklarzewicz, A. Samotus, K. Lewiński, *J. Chem. Soc., Dalton Trans.* (2002) 3587.
- [7] D. Matoga, J. Szklarzewicz, K. Lewiński, *Polyhedron* 27 (2008) 2643.
- [8] A. Roodt, J.G. Leipoldt, S.S. Basson, I.M. Potgieter, *Transition Met. Chem.* 15 (1990) 439.
- [9] S.S. Basson, J.G. Leipoldt, I.M. Potgieter, *Inorg. Chim. Acta* 87 (1984) 71.
- [10] S.S. Basson, J.G. Leipoldt, I.M. Potgieter, *Inorg. Chim. Acta* 90 (1984) 57.
- [11] J. Szklarzewicz, A. Samotus, N.W. Alcock, M. Moll, *J. Chem. Soc., Dalton Trans.* (1990) 2959.
- [12] B. Burda, J. Burgess, S.A. Parsons, A. Samotus, J. Szklarzewicz, *Transition Met. Chem.* 20 (1995) 291.
- [13] J. Szklarzewicz, *Transition Met. Chem.* 26 (2001) 189.
- [14] B. Nowicka, A. Samotus, J. Szklarzewicz, F.W. Heinemann, H. Kisch, *J. Chem. Soc., Dalton Trans.* (1998) 4009.
- [15] J. Szklarzewicz, A. Samotus, J. Burgess, J. Fawcett, D.R. Russell, *Transition Met. Chem.* 26 (2001) 1.
- [16] A. Roodt, S.S. Basson, J.G. Leipoldt, *Polyhedron* 13 (1994) 599.
- [17] J.G. Leipoldt, S.S. Basson, A. Roodt, I.M. Potgieter, *Transition Met. Chem.* 11 (1986) 323.
- [18] J. Szklarzewicz, A. Makuła, D. Matoga, J. Fawcett, *Inorg. Chim. Acta* 358 (2005) 1749.
- [19] J. Szklarzewicz, P. Paciorek, P. Zabierowski, K. Kurpiewska, M. Mikuriya, D. Yoshioka, *Polyhedron* 37 (2012) 35.
- [20] J. Szklarzewicz, K. Stadnicka, *Inorg. Chim. Acta* 393 (2012) 131.
- [21] P. Zabierowski, J. Szklarzewicz, K. Kurpiewska, K. Lewiński, W. Nitek, *Polyhedron* 49 (2013) 74.
- [22] A. Samotus, M. Dudek, A. Kanas, *J. Inorg. Nucl. Chem.* 37 (1975) 943.
- [23] R. Ahlrichs, H. Horn, A. Schaefer, O. Treutler, M. Haeser, M. Baer, S. Boecker, P. Deglmann, F. Furche, *Turbomole*, version 5.9.
- [24] M.J. Frisch, G.W. Trucks, H.B. Schlegel, G.E. Scuseria, M.A. Robb, J.R. Cheeseman, G. Scalmani, V. Barone, B. Mennucci, G.A. Petersson, H. Nakatsuji, M. Caricato, X. Li, H.P. Hratchian, A.F. Izmaylov, J. Bloino, G. Zheng, J.L. Sonnenberg, M. Hada, M. Ehara, K. Toyota, R. Fukuda, J. Hasegawa, M. Ishida, T. Nakajima, Y. Honda, O. Kitao, H. Nakai, T. Vreven, J.A. Montgomery, J.E. Peralta, F. Ogliaro, M. Bearpark, J.J. Heyd, E. Brothers, K.N. Kudin, V.N. Staroverov, R. Kobayashi, J. Normand, K. Raghavachari, A. Rendell, J.C. Burant, S.S. Iyengar, J. Tomasi, M. Cossi, N. Rega, J.M. Millam, M. Klene, J.E. Knox, J.B. Cross, V. Bakken, C. Adamo, J. Jaramillo, R. Gomperts, R.E. Stratmann, O. Yazyev, A.J. Austin, R. Cammi, C. Pomelli, J.W. Ochterski, R.L. Martin, K. Morokuma, V.G. Zakrzewski, G.A. Voth, P. Salvador, J.J. Dannenberg, S. Dapprich, A.D. Daniels, O. Farkas, J.B. Foresman, J.V. Ortiz, J. Cioslowski, D.J. Fox, *Gaussian 09*, Revision A.1.
- [25] A. Altomare, G. Cascarano, G. Giacovazzo, A. Guagliardi, M.C. Burla, G. Polidori, M. Camalli, *J. Appl. Crystallogr.* 27 (1994) 435.
- [26] G.M. Sheldrick, *Acta Crystallogr., Sect. A* 64 (2008) 112.
- [27] A. Ryniewicz, M. Tomecka, J. Szklarzewicz, D. Matoga, W. Nitek, *Polyhedron* 45 (2012) 229.
- [28] B. Nowicka, J. Burgess, S.A. Parsons, A. Samotus, J. Szklarzewicz, *Transition Met. Chem.* 23 (1998) 317.
- [29] J. Szklarzewicz, A. Gruszewska, *Transition Met. Chem.* 30 (2005) 27.